Silicon (2021) 13:4033–4045
https://doi.org/10.1007/s12633-020-00692-y

ORIGINAL PAPER

Ca-Ga Double Doping Strategy to Fabricate Hemostatic Mesoporous Silica Nanoparticles (MSN) with Antibacterial Activity

Sheng Ding[1] · Xiaohui Wei[1] · Kun Yang[1] · Song Lin[1] · Feng Tian[1] · Fan Li[1]

Received: 20 March 2020 / Accepted: 5 September 2020 / Published online: 18 September 2020

Abstract

Hemostatic materials with antibacterial properties become increasingly significant in military and civilian trauma care. In recent years, some advanced inorganic hemostatic materials (e.g. QuikClot, Combat Gauze, and WoundStat) have been reported to have their own drawbacks and side effects. In the study, the mesoporous silica nanoparticles (MSN) doped with calcium and gallium ($Ga_{0.5}$CaMSS) was explored for hemorrhage control together with good antibacterial properties. Transmission electron microscopy (TEM), the energy-dispersive X-ray spectrometer (EDS), Nitrogen gas adsorption-desorption measurements, X-Ray diffraction measurements (XRD) and the Fourier transform infrared (FTIR) spectra were used to characterize the coagulation-promoting surface chemistry, morphology and porous structure of the samples. The clotting blood tests (CBT), activated partial thromboplastin time (APTT) tests, prothrombin time (PT) tests, and thromboelastograph (TEG) analysis showed the much better hemostatic properties of the $Ga_{0.5}$CaMSN compared with the control and blank MSN. Besides, $Ga_{0.5}$CaMSN was found to have obvious antibacterial effect against both *S. aureus* and *E. coli*. Furthermore, the perfect biocompatibility of all samples was proved by hemolysis assay study and cytotoxicity test. Associated with the blood coagulation tests and antibacterial tests, it could be inferred that the stimulation of the blood coagulation and antibacterial activity of $Ga_{0.5}$CaMSN were attributed to the incorporation of calcium ions and gallium ions. The $Ga_{0.5}$CaMSN developed here can be a potent candidate for emergency treatment to control hemorrhage and wound infection pre-hospital.

Keywords Mesoporous silica nanoparticles (MSN) · Calcium · Gallium · Hemorrhage control · Antibacterial properties

1 Introduction

In modern war and pre-hospital period, excessive hemorrhage is still the main cause of death [1], and excessive hemorrhage accounts for 80% of early trauma deaths. Therefore, rapid hemorrhage control is essential for successful treatment. Meanwhile, the death of the wounded occurred in 5 days after injury is mainly due to the infection. It is reported that 2/3 to 3/4 of the post-war death is related to serious infections [2]. Therefore, the hemostatic materials with antibacterial properties will play an important role on treatments for the wounded pre-hospital.

Several clinical hemostatic agents have been applied to control hemorrhage, which were mainly divided into two parts: polymer materials (HemCon, Celox, Celox-D) and inorganic materials (QuikClot, WoundStat, and Combat Gauze). According to the data from US Army Institute of Surgical Research (USAISR), inorganic materials had better hemostatic performance than polymer materials [3, 4]. However, the advanced inorganic hemostatic materials used by US Army usually had their own side effects. For example, the residual of WoundStat resulted severe thrombus in the vessel and lung [5, 6]. Furthermore, WoundStat might cause severe inflammation of the blood vessels, and the damaged blood vessels could not be repaired. So WoundStat has been eventually banned by the U.S. military [7]. While the great exothermic reaction of QuikClot might cause severe thermal damage, which can lead to tissue necrosis and abnormal foreign-body reaction. It has been documented to cause thermal damage from second degree burns to the burns requiring skin grafts [8–11]. Combat Gauze might cause the more blood loss due to the poor adhesion and the residue preferred to

✉ Feng Tian
tianfeng62037@163.com

✉ Fan Li
vanadium_1981@163.com

[1] Institute of Medical Support Technology, Academy of Military Sciences, Tianjin 300161, People's Republic of China

remain in the wound [12, 13]. On the whole, the hemostatic result is that WoundStat is the best, Combat Gauze is the second and QuikClot is the weakest [6, 14, 15]. It is known that the core materials of WoundStat, Combat Gauze and QuikClot were aluminosilicate with porous structure, large specific surface area, and good adsorption capacity, which finally achieved rapid hemostasis. Recently, the mesoporous silica nanoparticles (MSN), which have controllable composition and modifiable surface besides the advantages of those aluminosilicate, were tried for hemostatic applications [16–18].

Calcium ion (Ca^{2+}), as one of the 13 coagulation factors involved in the coagulation reaction, has a significant influence on coagulation process. Ca^{2+} (Factor IV) can promote the blood coagulation reaction and help induce the activation and renewal of the endogenous coagulation cascade and other coagulation factors, accelerating the production of sufficient amounts of thrombin to support the early formation of fibrin, catalyzing the conversion of fibrinogen into fibrin in the blood, which is conducive to the chain polymerization of fibrin and the stability of blood coagulation [19, 20].

In recent years, it was found that gallium ion (Ga^{3+}) can treat localized infection, inhibit biofilm formation and impart bactericidal activity against both free living bacteria and biofilm cells [21, 22]. Ga^{3+} have shown significant antibacterial activity against both Gram-positive (*S. aureus*) and Gram-negative (*E. coli*) bacteria [23, 24]. Xu et al. [25] studied the antimicrobial effect of gallium nitrate on the infection in burn wound, and determined the minimum inhibitory concentration (MIC) of gallium nitrate on common bacteria in infected burns with Kit-WST, finding that gallium nitrate have good antibacterial activity against both Gram-positive and Gram-negative bacteria. The hemostatic activity of $Ga(NO_3)_3$ on ceasing blood flow from an open wound was studied by Goodley and Rogosnitzky [26, 27], which indicated the potential ability of the solution to significantly reduce clotting time [28]. Bauters et al. [29] found that gallium nitrate solution induced fibrinogen precipitation in whole blood samples by flocculation pathway to promote hemorrhage, which seemed to depend on the presence of gallium ions in the solution.

We have synthesized MSN with controllable pore sizes and studied the effect of pore size on the hemostatic performance of MSN [30]. However, the hemostatic mechanisms of Ca^{2+} and MSN are different, and there was no antibacterial activity for the primordial MSN. Hence here calcium and gallium ions were introduced to enhance the hemostatic properties and antibacterial properties of MSN, and the biocompatibility, hemostatic and antibacterial properties of the samples were evaluated.

2 Experimental Section

2.1 Materials

Tetraethyl orthosilicate (TEOS), Cetyltrimethyl ammonium bromide (CTAB), octane, L-Lysine, Methyl Methacrylate (MMA) and 2, 2′-Azobis (2-metrylpropionamide) dihydrochloride (AIBA) were all purchased from J&K Chemical. Calcium nitrate tetrahydrate [$Ca(NO_3)_2 \cdot 4H_2O$] and gallium nitrate hydrate (III) [$Ga(NO_3)_3 \cdot xH_2O$]were purchased from Sigma-Aldrich. All reagents were of reagent grade used without further purification. Deionized water was obtained by ion exchange.

2.2 Synthesis of MSNs

As reported by Chen et al. [30], Zhang Y et al. [31] and Nandiyanto et al. [32] with some modifications, the MSN were synthesized by the avesicle-organic template method in the oil/water phase. Briefly, a mixed solution was prepared by dissolving and heating 300 mg CTAB in 96 mL of deionized water at 70 °C in three-necked flask reactor with constant stirring. After the whole system was purged with nitrogen for 1 h, a clear solution could be achieved and then 9 mL octane were added to the surfactant solution. After the system was stirred for 30 min, 3.5 mL MMA, 66 mg L-lysine, 3000 mg TEOS and 0.84 mg AIBA were added to the system which was stirred at 800 rpm for 4 h under nitrogen at 70 °C. The MMA monomer was pre-washed with 5% NaOH to remove the polymerization inhibitor and then washed with distilled water prior to use. The resulting product was milky white with only one phase. Afterwards, the suspension was cooled to room temperature decanted for 12 h and then purified by centrifugation at 15,000 rpm for 15 min. The centrifuged particle was washed by anhydrous ethanol. Finally, in order to remove the organic template completely, the centrifuged particle was calcined at 600 °C for 5 h at a rate of 2 °C/min under atmospheric conditions.

The introduction of calcium or gallium ions into MSNs using 1 $mol \cdot L^{-1}$ of calcium nitrate solution or 0.5 $mol \cdot L^{-1}$ of gallium nitrate solution had been explored by our previous study. The suspension was stirred at room temperature for 1 h, and then the product was collected by suction filtration and dried at 80 °C. The product with the best hemostatic ability was selected by hemostatic tests including TEG, APTT, PT and CBT, so as to explore the hemostatic and antibacterial effect of the ternary compound system that composed of calcium ions, gallium ions and MSN.

2.3 Characterization

The inner microstructure of the samples prepared by suspending MSN in ethanol with ultrasound can be

Table 1 The particle sizes, pore sizes of different MSN according to TEM images, nitrogen adsorption tests

Sample	PSD(nm)	D_{TEM}(nm)	S_{BET}(m^2/g)	P_{BJH}(mL/g)	D_{BJH}(nm)
MSN	53.3 ± 7.0	12.5 ± 2.7	214.1	1.86	34.7
$Ga_{0.5}$MSN	52.9 ± 6.5	12.9 ± 2.3	149.5	1.02	27.3
CaMSN	52.2 ± 6.3	12.0 ± 2.1	73.6	0.77	41.6
$Ga_{0.5}$CaMSN	53.4 ± 5.8	12.9 ± 2.1	66.2	0.70	42.3

Particle size distribution (PSD) was decided by measuring the diameters of particles under TEM (Fig. 1). D_{TEM} was the pore diameter calculated by measuring the pore diameters under TEM. S_{BET} was the specific surface area evaluated by the BET model. P_{BJH} was the total internal pore volume measured from N_2 adsorption. D_{BJH} was the pore diameter evaluated by the BJH theoretical model

observed by transmission electron microscopy (TEM, JEOL JEM-2100F) working at 200 kV. And then the assessment of the composition of the samples can be achieved using the energy-dispersive X-ray spectrometer (EDS). Specific surface area, the total volume and the pore diameter are determined by N_2 gas adsorption-desorption method through the Micromeritics porosimeter (Auto-sorb-iQA3200–4, Quantatech Co, USA). Small and wide angle XRD measurements were carried out by using the X-ray diffractometer (D8 Advance, Buker) with Cu-Kα(λ = 0.15604) radiation at 30 mA and 30 kV. The small angle XRD patterns were collected in the 2θ range between 0.5° and 10° with the step size of 0.02° and the counting time of 4° /min. While the wide angle XRD patterns were collected in the 2θ range between 5° and 80° with the step size of 0.02° and the counting time of 4° /min. The FT-IR spectra of the synthesized samples were measured on the Fourier transform infrared spectrometer (Nicolet 380, Thermo, USA) within the 4000-400 cm^{-1} wavelength range.

3 Determination of Clotting Activity of Different MSN

3.1 Thromboelastograph Analysis (TEG)

Thromboelastograph Analyzer (TEG, CFMS LEPU-8800, China) was used to analyze citrated rabbit whole blood clotting kinetics. Before testing, the samples were dried at 80 °C to remove moisture. 10 mg of sample were added into 1 mL citrated rabbit whole blood. Using the vortex mixer to get the homogeneous mixture and then 340 μL of the mixture was added to the coagulation cup at 37 °C. Then after 20 μL of 0.2 $mol{\cdot}L^{-1}$ $CaCl_2$ was also added to the coagulation cup, the coagulation cups were immediately tested to obtain the relevant parameters including reaction time (R), angle (α) and maximum amplitude (MA). Citrated rabbit whole blood without samples was used as a blank control group, and each group of samples was tested repeatedly three times.

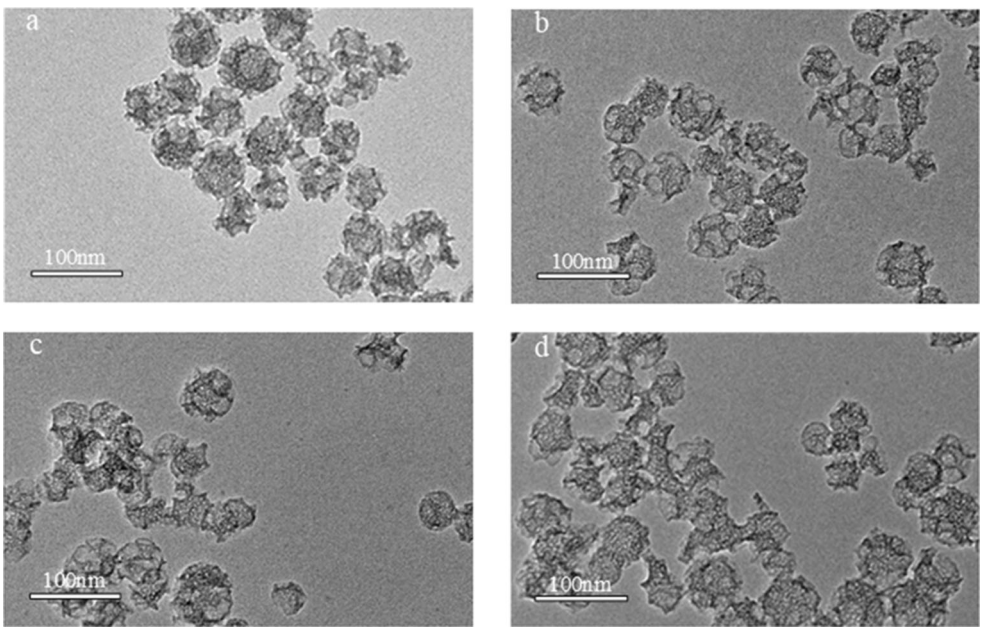

Fig. 1 TEM photographs of MSNs with different components: **a** MSN; **b** $Ga_{0.5}$MSN; **c** CaMSN; **d** $Ga_{0.5}$CaMSN

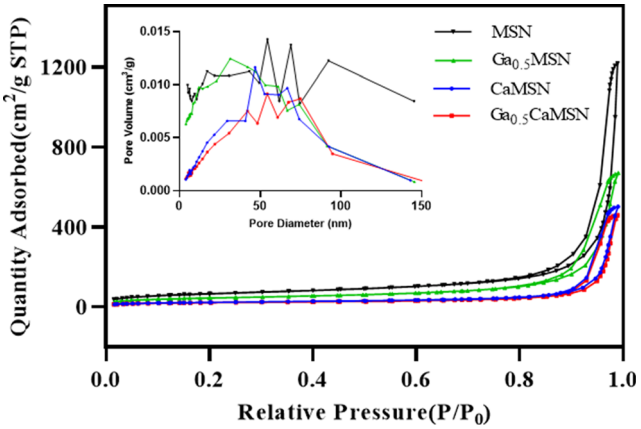

Fig. 2 Nitrogen adsorption/desorption isotherms and BJH pore size distribution of MSN, $Ga_{0.5}$MSN, CaMSN, $Ga_{0.5}$CaMSN

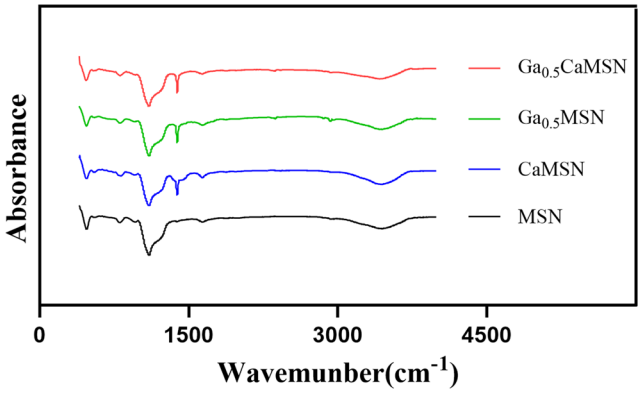

Fig. 3 FTIR spectra of MSN with different components: (A) MSN, (B) CaMSN, (C) $Ga_{0.5}$MSN, (D) $Ga_{0.5}$CaMSN

3.2 Activated Partial Thromboplastin Time (APTT) and Prothrombin Time (PT) Tests

APTT and PT are two basic clinical standard coagulation tests. APTT can reflect the intrinsic coagulation pathway while PT is associated with extrinsic pathway. Blood samples mixed a one-tenth volume of with 3.8% sodium citrate were from New Zealand rabbits. After the centrifugation of the blood samples at 2500 g for 15 min, the platelet poor plasma (PPP) was obtained by collecting the supernatant.

For the APTT assay, 0.1 mL of APTT reagent and 0.1 mL of the platelet poor plasma were added to the test tubes with 2 mg selected samples. After incubation at 37 °C in a water bath for 3 min, 0.1 mL of 0.025 mol·L^{-1} pre-warmed $CaCl_2$ were added in the test tube and APTT was measured simultaneously.

For the PT assay, 0.1 mL of the platelet poor plasma were added to the test tubes with 2 mg selected samples. After incubation at 37 °C in a water bath for 3 min, 0.1 mL of pre-warmed PT reagent were added in the test tube and PT was measured simultaneously.

3.3 Clotting Blood Tests (CBT)

The CBT test based on reported literature is one of the basically hemostatic tests which can directly reflect and evaluate the hemostatic ability [33]. 20 mg of each sample were added to a glass test tube and incubated at 37 °C in a water bath for 3 min. 1 mL citrated rabbit whole blood was added to the glass test tube and incubated for 1 min. Then 500 μL of 0.025 mol·L^{-1} $CaCl_2$ was added, and CBT was measured simultaneously. The citrated rabbit whole blood without sample was used as control group, and each sample was repeatedly measured 3 times.

Table 2 The EDS results of $Ga_{0.5}$MSN, CaMSN, $Ga_{0.5}$CaMSN

Element (Wt%) Sample	Si	O	Ga	Ca
MSN	56.48	43.52	0	0
$Ga_{0.5}$MSN	55.98	41.40	2.62	0
CaMSN	55.48	42.67	0	1.85
$Ga_{0.5}$CaMSN	55.75	39.95	2.57	1.73

3.4 Antibacterial Tests

The antibacterial property of the samples was tested by the inhibition zone method. *S. aureus* and *E. coli* were used for the antibacterial activity analysis. Before the assay, the same amount of the samples was pressed by a stainless stamper to obtain a 7 mm diameter nummular type, and then irradiated with ultraviolet rays for 3 h for sterilization. *S. aureus* and *E. coli* were grown on liquid nutrient agar media and activated for 24 h at 37 °C in the electric thermostatic incubator prior to the assay. *S. aureus* and *E. coli* were diluted with PBS buffer to 10^8 CFU/mL and 10^6 CFU/mL, respectively. 500 μL of diluted bacteria suspension was coated on the surface of solid medium according to the K-B method. The nummular samples were placed on the center of the solid medium with bacteria incubated at 37 °C, and then the inhibition zones were measured after 24 h. The diameter of the inhibition zone was used as the evaluation of the antibacterial property.

3.5 In Vitro Hemolysis Assay

Hemolysis assay was used to evaluate the hemocompatibility of the samples based on the reported literature [34]. 2 mL citrated rabbit whole blood mixed with 8 mL PBS was centrifuged at 2500×g for 15 min to collect erythrocytes. 1 mL erythrocytes were added to 9 mL PBS to obtain erythrocyte suspension. And then 1 mg samples were added to 1 mL erythrocyte suspension, which were used as treatment groups. 1 mL erythrocyte suspension were used as negative control groups while 0.1 mL erythrocyte suspension mixed with

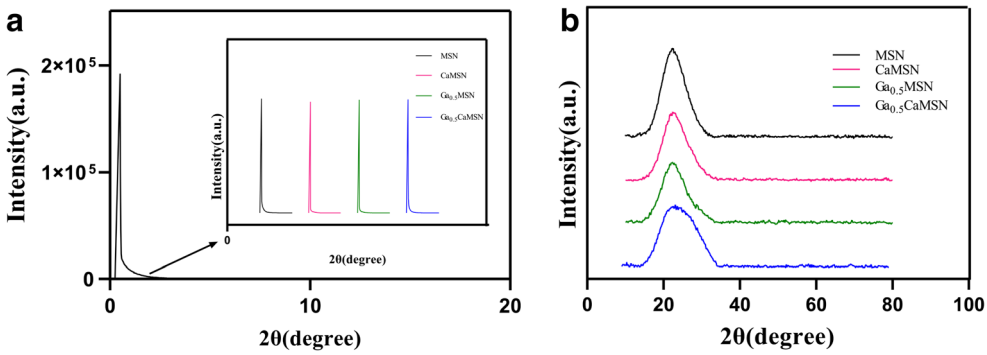

Fig. 4 The small-angle (**a**) and wide-angle (**b**) XRD patterns of MSN with different components (MSN, CaMSN, $Ga_{0.5}$MSN and $Ga_{0.5}$CaMSN)

0.9 mL deionized water without samples were used as positive control groups. After incubation at 37 °C for 1 h, treatment and control groups were centrifuged at 2000×g for 15 min to obtain the supernatant. The absorbance of the supernatant was measured at 540 nm by using ultrviolet spectrophotometer, the hemolysis ratio was calculated according to Formulae:

$$Hemolysis\ ratio = \frac{ODsample - ODnegative}{ODpositive - ODnegative} \times 100\%$$

3.6 Cytotoxicity Test

Because of hemostatic mainly used on skin, endothelial cells were chosen to study. In order to analyze the biocompatibility and the influence of different dosages of the samples on the cells, the low concentration of 320 μg/mL samples and the high concentration of 640 μg/ml samples in PBS were set [29]. The endothelial cells were transplanted into a 96-well plate at 10,000 cells/well and cultured for 24 h. Then 200 μL of 320 μg/mL and 640 μg/mL samples in PBS were added respectively and incubated for 24 h. While 200 μL of PBS was added and incubated for 24 h as the control group.

CCK-8 toxicity detection: After discarding the liquid in the well and washing the cells several times with PBS, 100 μL of serum-free medium and 10 μL of CCK-8 solution were added to each well and incubated in the cell incubator for 1 h. The absorbance intensity was detected at 450 nm with the microplate reader.

Staining of dead/live cell: After discarding the liquid in the well and washing the cells several times with PBS, 50 μL dead/live cell staining solution were added and incubated for 20 min at room temperature. Images of live (green fluorescence) and dead (read fluorescence) cells were obtained with the fluorescence microscope.

3.7 Hemostatis in the Mouse Tail Amputation Model

The mice (30–35 g, male) randomly divided into five groups were prepared to conduct the mouse tail amputation model assay [35]. The mice were anesthetized by injecting 3% wt% pentobarbital sodium (50 mg/kg) intraperitoneally and fixed on the surgical board. After the tail was sterilized, 2/3 of its length was cut down using surgical scissors. The wound was allowed to bleed freely for 5 s to ensure normal blood loss, then the wound was covered with the sterilized samples (Gauze, $Ga_{0.5}$MSN, CaMSN, $Ga_{0.5}$CaMSN) used as the treatment groups under slight compression. The wound without samples was used as the negative group. Then the pressure was removed about 10–15 s and the bleeding was observed. If there was no bleeding in 30s,

Table 3 In vitro thromboelastograph results of the control and different MSNs (MSN, $Ga_{0.5}$MSN, CaMSN, $Ga_{0.25}Ca_{0.5}$MSN, $Ga_{0.5}$CaMSN). *, # meant significant difference compared to the control and MSN, respectively ($p < 0.05$)

Sample	R(min)	a(degree)	MA(mm)
control	11.8 ± 0.7	26.8 ± 0.8	61.7 ± 0.2
MSN	6.9 ± 0.3*	53.4 ± 5.1*	67.3 ± 2.1*
$Ga_{0.5}$MSN	5.4 ± 0.2*#	65.7 ± 1.0*#	64.3 ± 0.4*
CaMSN	4.5 ± 0.3*#	73.3 ± 3.5*#	73.5 ± 3.6*#
$Ga_{0.25}Ca_{0.5}$MSN	5.3 ± 0.2*#	60.4 ± 1.1*#	61.3 ± 0.3#
$Ga_{0.5}$CaMSN	4.2 ± 0.3*#	65.5 ± 0.9*#	67.2 ± 1.5*

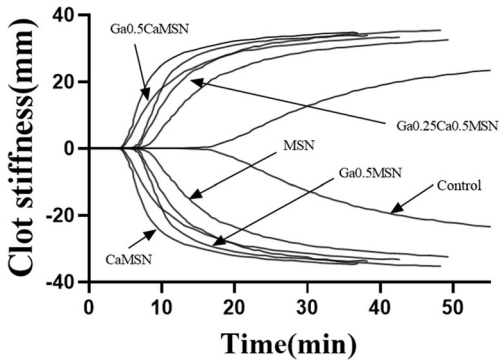

Fig. 5 The representative thromboelastograph plots of the control and MSNs (MSN, $Ga_{0.5}$MSN, CaMSN, $Ga_{0.5}$CaMSN)

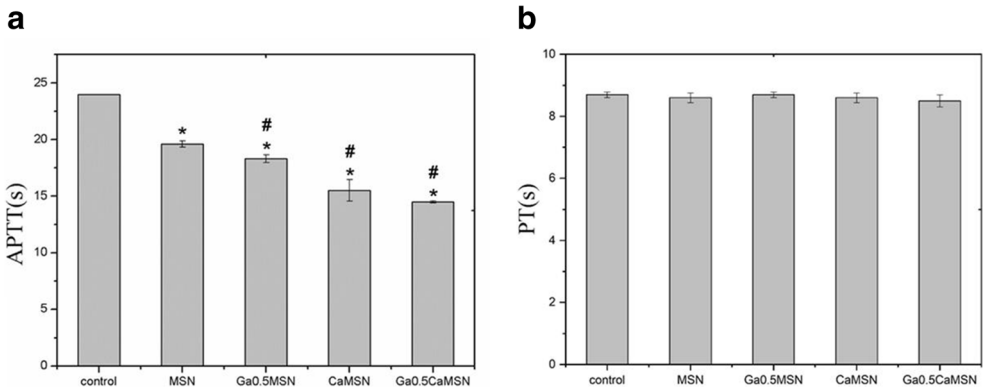

Fig. 6 Changes in (**a**) activated partial thromboplastin time (APTT) and **b** prothrombin time (PT) of MSNs (MSN, $Ga_{0.5}$MSN, CaMSN, $Ga_{0.5}$CaMSN) in PPP of rabbit. *, # meant significant difference compared to the control and MSN, respectively ($p < 0.05$)

the hemostasis was thought to be successful and hemostatic time and blood loss were recorded.

3.8 Hemostasis in Rabbit Femoral Artery

In this study, a model of hemostasis in rabbit femoral artery was used to test and evaluate the hemostatic capacity of $Ga_{0.5}$CaMSN. Adult male New Zealand white rabbits with the body weight of 2.5 ± 0.2 kg were randomly assigned into 2 groups. After ultraviolet sterilization, $Ga_{0.5}$CaMSN was used as the experimental group, and the gauze was used as the control. The animals had to be fasted the day before the experiment, except the water.

Preoperative anesthesia was performed by intravenous injection of 45 mg/kg pentobarbital sodium in the animals. A longitudinal incision about 5 cm was made at the left anterior femoral root of the rabbit and the femoral artery was separated by blunt tweezers from the surrounding muscles. During the experiment, local anesthesia and tissue infiltration of 10 mg/kg lidocaine injected into the incision and perivascular muscles can prevent vasospasm. The femoral artery was cut off by the scalpel. After natural bleeding for 3 s, 2 g $Ga_{0.5}$CaMSN was applied immediately over the location of wound with 30 N

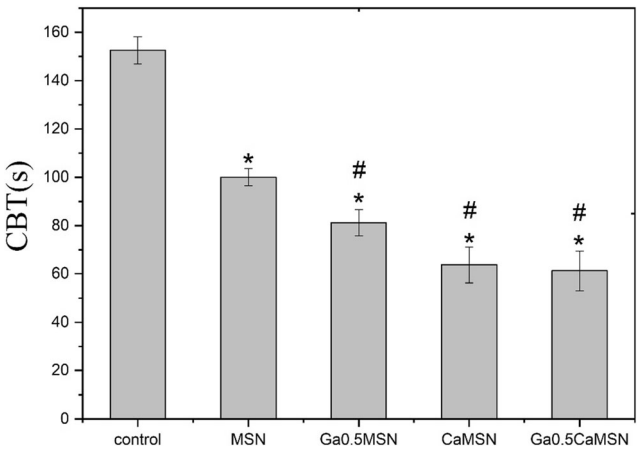

Fig. 7 CBTs for the control and MSNs: MSN, $Ga_{0.5}$MSN, CaMSN, $Ga_{0.5}$CaMSN. *, # meant significant difference compared to the control and MSN, respectively ($p < 0.05$)

manual compression. Bleeding was observed each 15 s and when it could not be observed on the surface of the material and remained unchanged for 30s, the bleeding was considered to have been completely stopped. The hemostasis experiment was completed, and the hemostasis time was recorded. After the hemostasis test was completed, the wound was rinsed with normal saline and was sutured. Animals were observed within 24 h, and then the surviving animals were sacrificed with an overdose of pentobarbital sodium.

3.9 Statistical Analysis

All data given in this study were expressed as mean ± standard deviation. The significance of statistical difference was determined by using a one-way analysis of variance (ANOVA). Results were considered to be statistically significant at $p < 0.05$. Each test was repeated at least three times.

4 Results and Discussion

The morphology of MSNs with different components were analyzed by TEM. As shown in Fig. 1, the synthesized MSNs all had a monodispersed spherical shape with similar sizes. The mean pore sizes and particle sizes of MSNs were about 12 nm and 50 nm respectively. According to TEM images, the pore channels appeared to be radical and some MSNs appeared to be hollow, which revealed existence of the pores both on the particle surface and within the particle. The mean pore sizes and particle diameters were presented in Table 1. It revealed that the introduction of ions had little effect on the morphology of the samples. TEM showed the large pore size of successfully synthesized MSNs which could promote hemostasis as reported.

N_2 adsorption-desorption isotherms were measured at 77.4 K and the samples were degassed at 573 K under nitrogen for 12 h prior to analysis. The N_2 adsorption-desorption isotherms of the synthesized samples were measured and shown in Fig. 2, which were typical type IV isotherm with a H_1 hysteresis according to the IUPAC classification. It was in

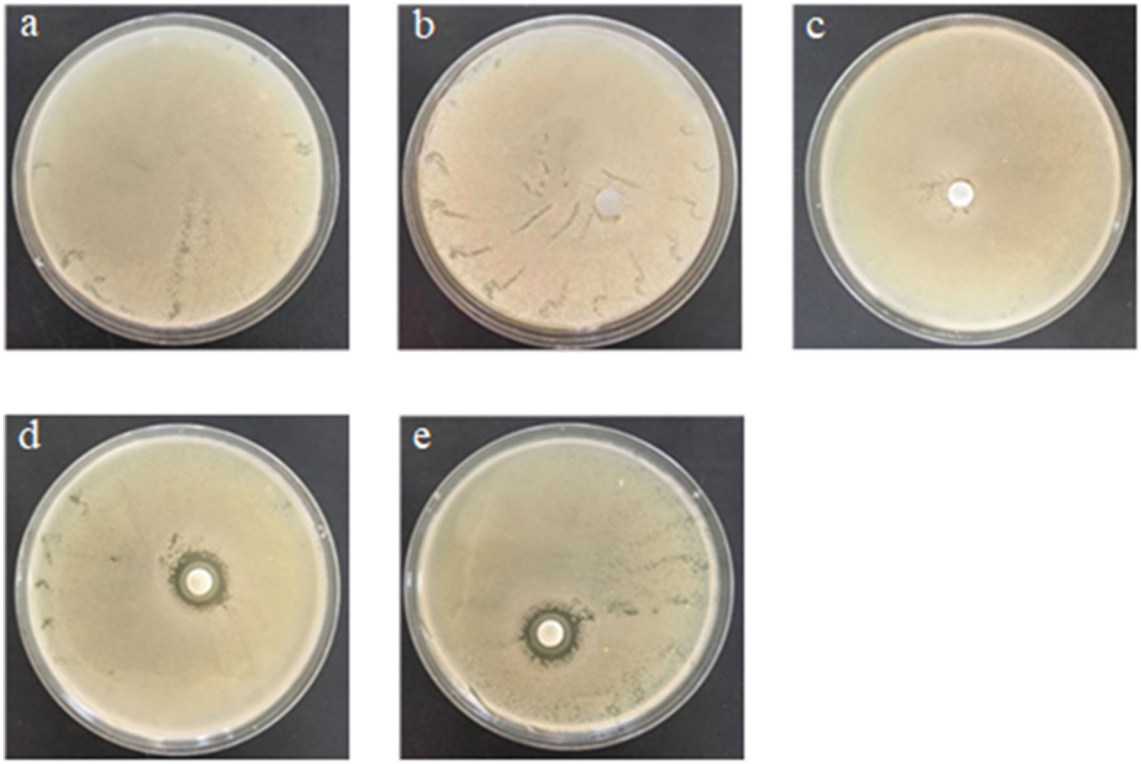

Fig. 8 The inhibition zones of (**a**) control, **b** MSN, **c** CaMSN, **d** $Ga_{0.5}$MSN, **d** $Ga_{0.5}$CaMSN against *S. aureus*

accord with the characteristic of mesoporous materials, proving the mesoporous structure of the samples. The data of the BET specific area (S_{BET}), the BJH Pore volume (P_{BJH}) and the BJH pore diameter (D_{BJH}) were given in Table 1. Compared with the pore sizes measured by TEM, the BJH pore diameters were much bigger, which could be concluded that MSNs had

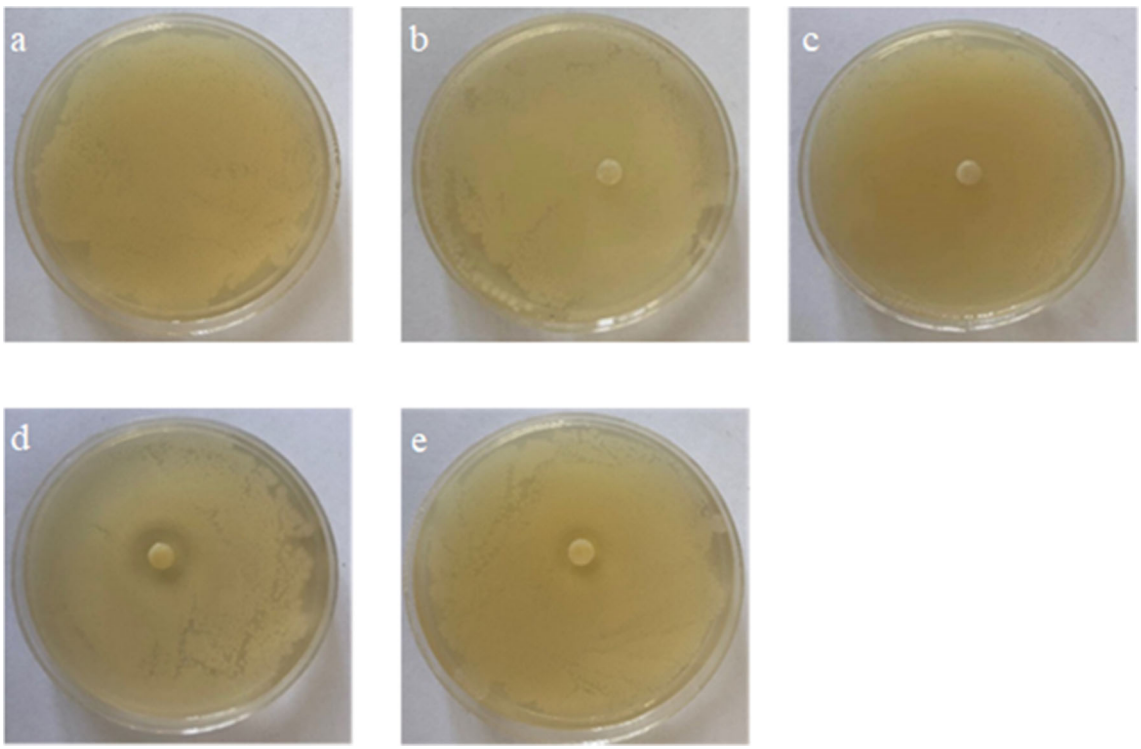

Fig. 9 The inhibition zones of (**a**) control, **b** MSN, **c** CaMSN, **d** $Ga_{0.5}$MSN, **e** $Ga_{0.5}$CaMSN against *E. coli*

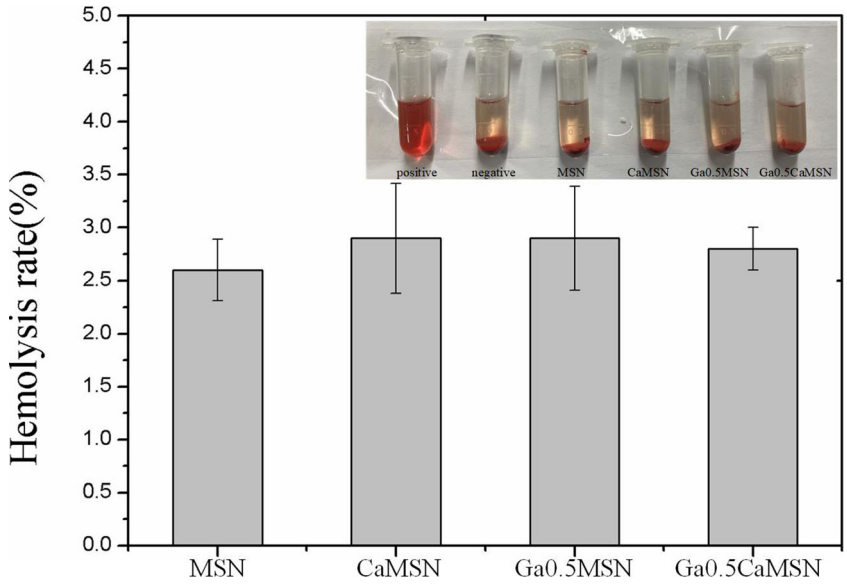

Fig. 10 Hemolysis ratio of (a) MSN, (b) $Ga_{0.5}MSN$, (c) CaMSN, (d) $Ga_{0.5}CaMSN$

interparticle and hollow void together with the view of TEM images. MSNs with interparticle and hollow void had the positive effect on hemostasis. The P_{BJH} and S_{BET} decreased with the introduction of the ions. There was little change on the D_{BJH} of Ca-containing-MSN compared with the MSN. While with only the gallium introduced, the D_{BJH} of $Ga_{0.5}MSN$ decreased. The reason might be that some of the pores within the particle in $Ga_{0.5}MSN$ adsorbed the gallium in view of TEM images. The changes of the D_{BJH} might be linked to the pores within the MSNs. In conclusion, associated with the TEM images, the influence of the introduction of ions on the structure was mainly reflected in the specific surface area and pore volume. However, the introduction of ions had little effect on the pores existed on the particle surface, which was the important factor of the coagulation properties.

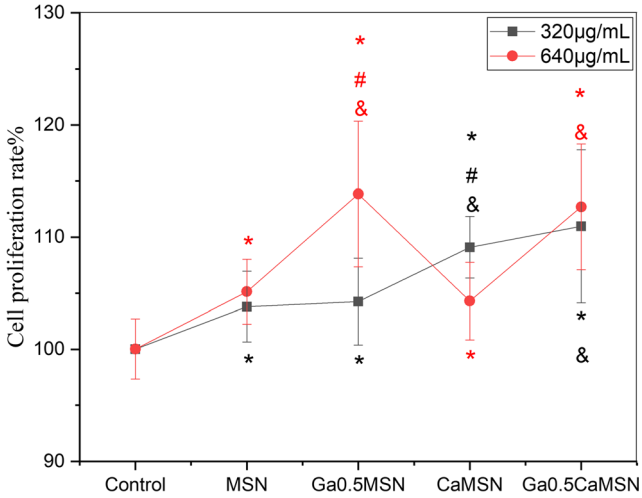

Fig. 11 CCK-8 toxicity detection of MSNs at the low concentration (320 μg/mL) and the high concentration (640 μg/mL): Black line and red line represented the low concentration (320 μg/mL) and the high concentration (640 μg/mL), respectively, * meant significant difference compared with the control group, # meant significant difference between the same sample at different concentrations, & meant significant difference compared with the MSN at the same concentration ($P < 0.05$)

EDS can qualitatively assess the composition of the samples. As shown in Table 2, the existence of calcium and gallium ions could be confirmed. The MSN loaded with ions might be due to the adsorption effect produced by the mesoporous channels and the large pore sizes. Another reason might be the highly active hydroxyl groups present on the surface of the MSN, which can be dehydrogenated to form the SiO^- in a negative ion state and then had the attraction to the cation.

In order to detect the changes of surficial chemical structure in the particle, FTIR spectroscopy analysis of the samples was conducted. As presented in Fig. 3, with the introduction of the ions, the NO_3- appeared at around 1350 cm^{-1}, which indicated the successful load with ions associated with the EDS. Despite the appearance of NO_3- at around 1350 cm^{-1}, there were no other changes, indicating the introduction of the ions did not significantly influence the surface state of MSNs. There were many Si-OH functionalities on the surface of the samples (3200–3400 cm^{-1}) and absorption peaks centered at around 1100 cm^{-1} corresponding to the Si-O-Si asymmetric stretching mode and Si-O-Si bending at approximately 468 cm^{-1} of the MSNs.

Due to the stronger coagulation reaction and lower toxic reaction caused by the amorphous silica than crystalline silica [36], the amorphous silica was chosen to be used in hemostasis and the XRD pattern of MSNs were recorded to determine the crystal form. As shown in Fig.4(a), the small-angle XRD patterns of the MSNs powders with or without calcium and gallium all had only one peak appeared at about 1°, which proved that the prepared mesoporous silica nanoparticles were ordered, revealed that all the samples were totally amorphous

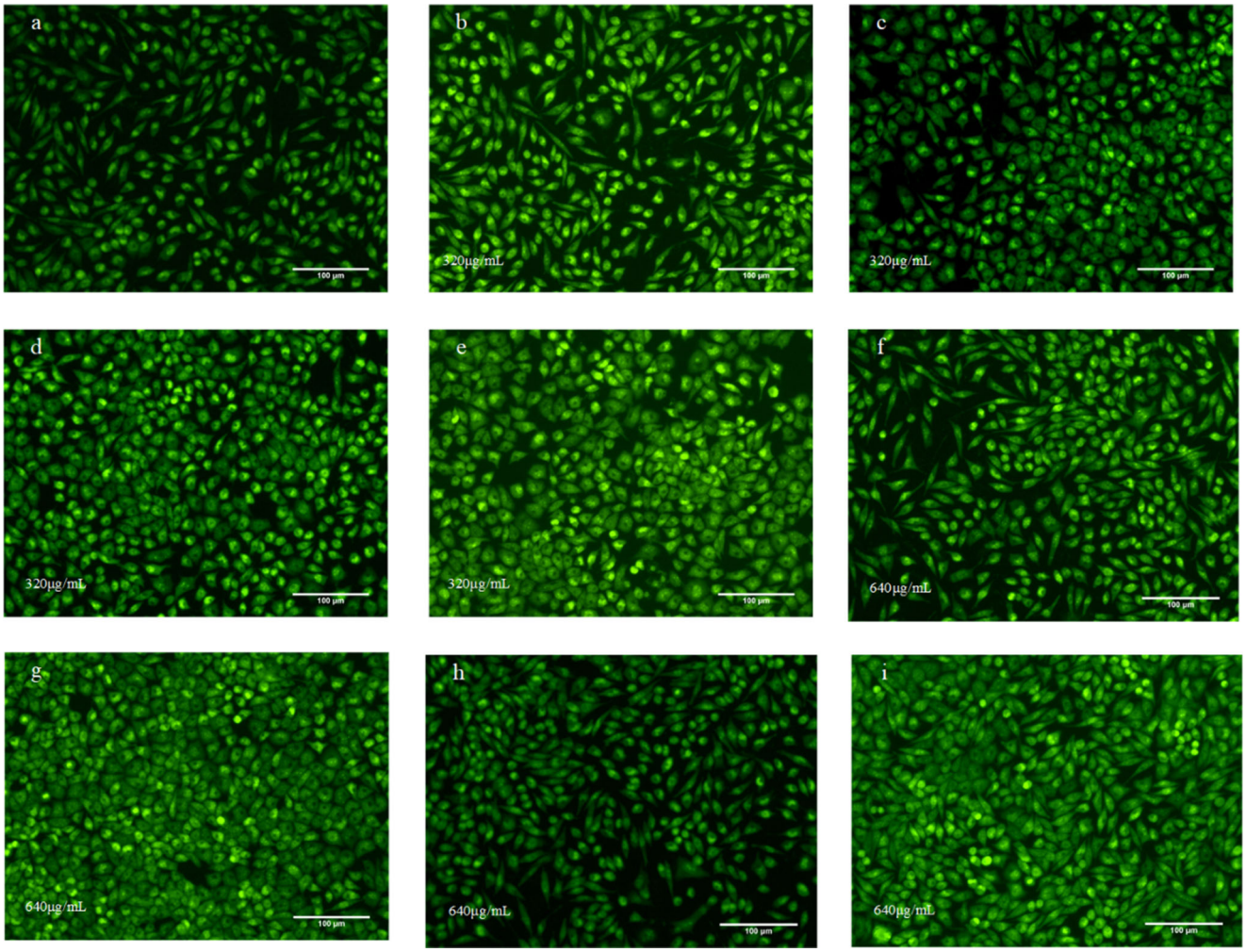

Fig. 12 The dead/live cell staining chart. **a** showed the dead/live cell staining chart of the control. **b**-**e** and **f**-**i** showed the dead/live cell staining chart of MSN, $Ga_{0.5}$MSN, CaMSN, and $Ga_{0.5}$CaMSN at low concentration (320 μg/mL) and the high concentration (640 μg/mL), respectively

and represented the pore existence. As shown in Fig.4(b), there were no diffraction peaks with crystal structure characteristics in the XRD wide-angle diffraction region, where only one peak appeared at about 10°-40°, which indicated that the calcium and gallium were all present in an amorphous form in MSN. Besides, the XRD pattern of MSNs indicated that calcium and gallium did not influence the structure of MSN.

Thromboelastograph Analyzer is an instrument which can diagnose blood disorders comprehensively and effectively by monitoring the change in the viscoelasticity of blood during blood coagulation [37]. The main parameters of TEG to quantify the clot formation are R, α and MA. R is the coagulation reaction time, which indicates the time from the initiation of the coagulation system to the onset of fibrin clot formation and reflects the combined effect of clotting factors. α is the angle between the horizontal line and the tangent from clot formation point to the maximum curvature of the curve, which is associated with the rate of coagulation. MA represents the maximum strength of the blood clot.

According to the previous study, the hemostatic and antibacterial effect of the ternary compound system that composed of calcium ions, gallium ions and MSN was explored. The thromboelastograms for rabbit blood containing MSNs with different compositions are depicted in Fig. 5 and the detailed data are listed in Table 3. It was found that MSN directly mixed with the optimal concentrations of calcium ions and gallium ions ($Ga_{0.5}$CaMSN) had a nice and acceptable hemostatic property. Compared with the control and MSN, $Ga_{0.5}$CaMSN had a significant difference. Although the α of $Ga_{0.5}$CaMSN decreased compared with CaMSN, R and MA had no significant difference. In order to enable MSN to have antibacterial properties, $Ga_{0.5}$CaMSN was selected for further investigation.

The clinical standard coagulation tests, APTT and PT, reflect the intrinsic coagulation pathway and the coagulation extrinsic pathway. As shown in Fig. 6(a), $Ga_{0.5}$CaMSN could still effectively reduce the APTT value compared with the control, MSN and $Ga_{0.5}$MSN, showing the potential

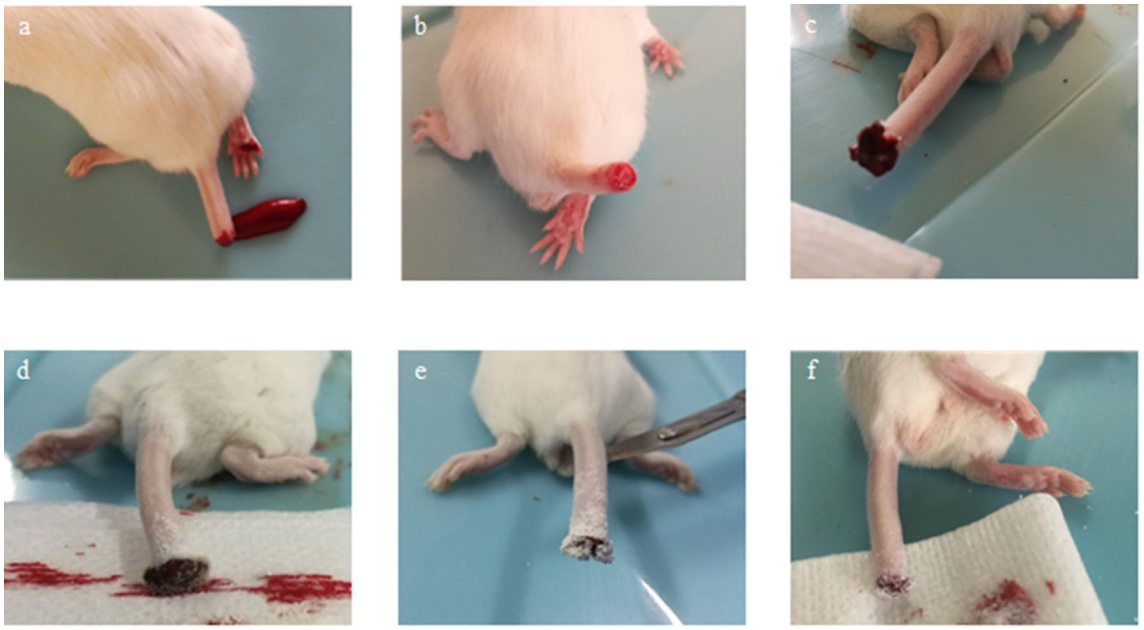

Fig. 13 Hemostasis tests in mouse tail amputation hemorrhage: **a** Control, **b** Gauze, **c** MSN, **d** $Ga_{0.5}$MSN, **e** CaMSN, **f** $Ga_{0.5}$CaMSN

hemostatic ability. APTT results indicated that all of the samples resulted in a significant activation of intrinsic pathways of the coagulation cascade since the APTT values were significantly diminished with respect to the control. However, there was no significant difference in the PT values of the samples shown in Fig. 6(b). All the samples showed approximately the same effect on PT values of that of the control, suggesting that MSNs had no significant influence on extrinsic coagulation pathway.

CBT is a basic hemostatic test which can directly reflect the hemostatic ability of the samples. Figure 7 shows that the CBT for $Ga_{0.5}$CaMSN (61.3 ± 8.2 s), CaMSN (63.8 ± 7.4 s) and $Ga_{0.5}$MSN (81.3 ± 5.4 s) are clearly shortened compared with the control (152.5 ± 5.6 s) and MSN (100.0 ± 3.5 s). The results of CBT which were in accordance with the results of TEG and APTT tests indicated that the introduction of calcium ions and gallium ions can enhance the hemostatic performance of MSN. Especially, the selected ternary compound system, $Ga_{0.5}$CaMSN could still have an acceptable hemostatic ability.

Bacterial infection can seriously influence the success of the first aid in wartime and the post-war treatment, threatening the health of the wounded. Therefore, the development of hemostatic materials with antibacterial effect will play an important role in the treatment of the wounded. As shown in Figs. 8 and 9, the results of inhibition zones of antibacterial activity could be measured. The diameter of the inhibition zones of $Ga_{0.5}$MSN and $Ga_{0.5}$CaMSN against *S. aureus* were 3.7 mm and 3.2 mm respectively. The diameter of the inhibition zones

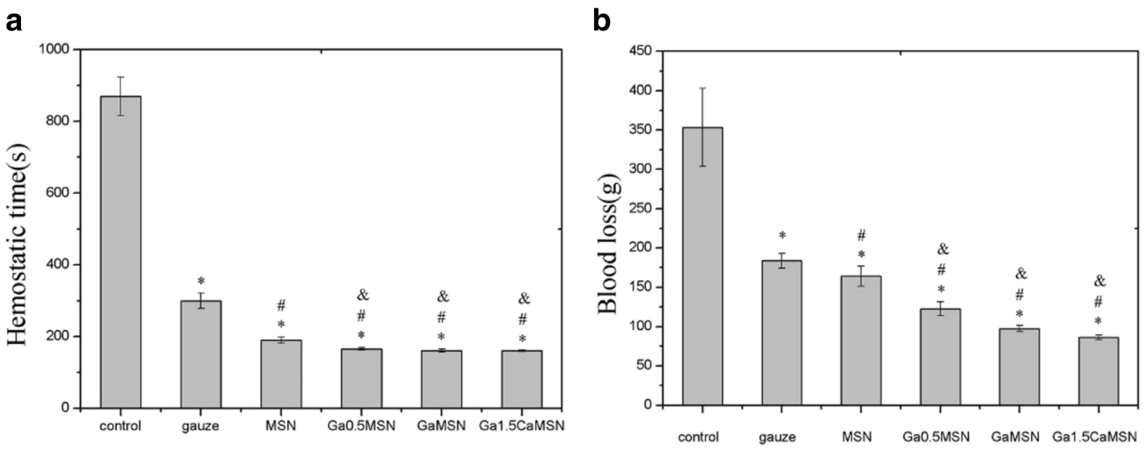

Fig. 14 The hemostatic time (**a**) and blood loss weight (**b**) of the control, gauze, MSN, $Ga_{0.5}$MSN, CaMSN, $Ga_{0.5}$CaMSN. All data were expressed as mean ± SD; $n \geq 3$. *, #, & meant significant difference compared to control, MSN and gauze, respectively ($p < 0.05$)

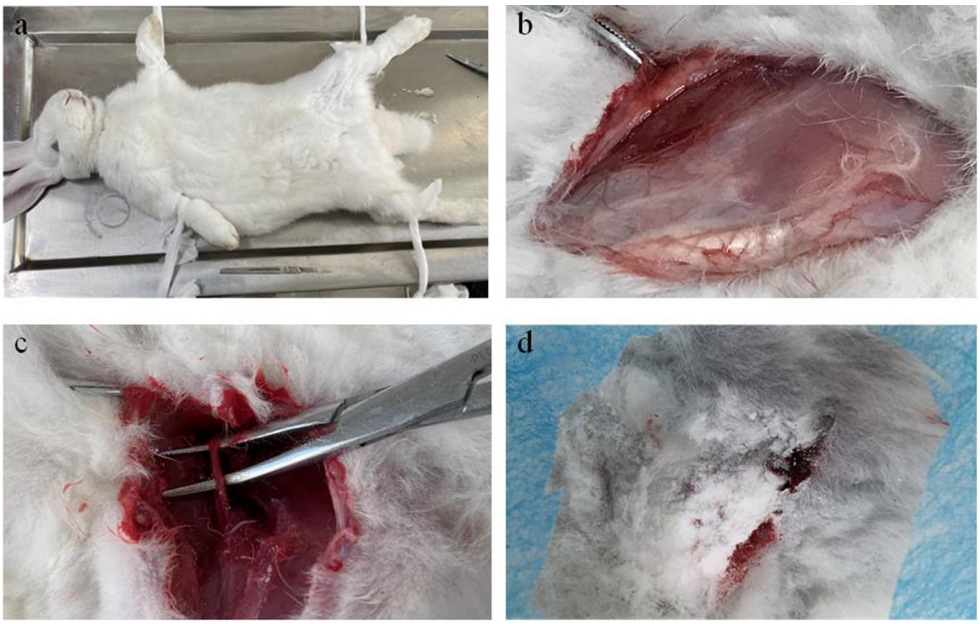

Fig. 15 Hemostasis in rabbit femoral artery injury: **a** Preoperative anesthesia and fixation of rabbits; **b** Opened skin and muscle to achieve a complete cut in femoral artery; **c** Separation and severing of rabbit femoral artery; **d** Bleeding stopped status after hemostasis

of $Ga_{0.5}$MSN and $Ga_{0.5}$CaMSN against *E. coli* were 3.8 mm and 2.7 mm respectively. While MSN and CaMSN had no anti-bacterial property.

Compared with non-Ga-containing MSN, Ga-containing MSN demonstrated a potent antibacterial effect against both pathogens which might be attributed to the presence of Ga^{3+}, indicating that the introduction of Ga^{3+} could enhance the antibacterial properties of the material. Besides, considering the diameter of the inhibition zones of Ga-containing MSN against *S. aureus* and *E. coli* had no significant difference while the concentration of *S. aureus* suspension was much higher, it could be speculated that Ga-containing MSN played a more significant antibacterial impact against *S. aureus* than against *E. coli*. Therefore, the selected $Ga_{0.5}$CaMSN could have a significant antibacterial effect and hemostatic property at the same time.

The hemolysis rate is an important parameter to evaluate the hemocompatibility of hemostatic materials which may come into the direct contact with vascular blood flow. According to the reported literature, the hemolysis rate of hemostatic materials is required to be less than 5% [34]. Therefore, hemolysis assay was conducted to evaluate the different samples. As shown in Fig. 10, the hemolysis rates of the samples were all far more less than 10%, indicating that the samples had acceptable hemocompatibility and the introduction of ions had no effect on the hemocompatibility of the samples.

The results of CCK-8 cytotoxicity test were shown in Fig.11. The cell proliferation rate of the CaMSN was significantly reduced at the high concentration compared with at the low concentration and the cell proliferation rate of $Ga_{0.5}$MSN was significantly increased at the high concentration than at the low concentration; while the cell proliferation rate of MSN and $Ga_{0.5}$CaMSN had no significant difference at different concentrations, showing the more stable biocompatibility. Compared with the pure MSN, MSN doped with calcium or gallium ions would better promote cell proliferation. The CCK-8 cytotoxicity test showed that all the samples could promote cell proliferation with good biocompatibility. And $Ga_{0.5}$CaMSN had the best effect of promoting the cell proliferation compared with others at different concentrations, which would not be influenced by the dosages.

As shown in Fig. 12, dead/live cell staining results showed that all the samples had good biocompatibility and could promote cell proliferation; while the $Ga_{0.5}$CaMSN showed the best effect of promoting cell proliferation, and it would not be influenced by the change of dosage. These results were consistent with the CCK-8 cytotoxicity test results.

In this experiment, the tail of mice was cut down by surgical scissors and with resultant hemorrhagic gushing bleeding. After free bleeding for 5 s, about 40 mg MSNs were applied over the site of injury, which could adhere tightly to the wound surface and seal bleeding quickly (Fig. 13). The hemostatic time is shown in Fig. 14(a). Compared with the gauzes (300.0 ± 21.8 s) and the negative control group (870.0 ± 53.5 s), the other samples can significantly shorten the hemostatic time ($p < 0.05$). The hemostatic time for $Ga_{0.5}$MSN (165 ± 8.8 s), CaMSN (160.0 ± 4.7 s) and $Ga_{0.5}$CaMSN (160.0 ± 2.6 s) are shorter than MSN (190.0 ± 8.5 s). As shown in Fig. 14(b), blood losses for CaMSN (97.6 ± 3.6 g) and $Ga_{0.5}$CaMSN (86.4 ± 3.0 g), MSN (164.3 ± 12.6 g), $Ga_{0.5}$MSN (122.7 ± 8.8 g) are significantly lower than the gauzes (183.7 ± 9.3 g) and the negative control group (353.3 ± 49.9 g). And the improved hemorrhage performance might be due to that calcium and gallium were efficient for the enhancement of the early stage of hemostasis including the

acceleration of blood coagulation, platelet activation, and clot formation when directly applied to the open wound. In addition, all the mice treated after 1 day with the samples survived.

The previous experimental results showed that $Ga_{0.5}$CaMSN had ideal hemostatic and antibacterial performance. In order to further verify the hemostatic performance of $Ga_{0.5}$CaMSN, the rabbit femoral artery hemorrhage model was used to evaluate the hemostatic effect in response to fatal hemorrhage in vivo (Fig. 15).

Compared with the gauze (342.3 ± 7.4 s), $Ga_{0.5}$CaMSN significantly reduced the hemostasis time (146.7 ± 10.4 s) ($p < 0.05$), which was consistent with the previous results in vitro coagulation test. The results showed that the blood loss was significantly reduced by $Ga_{0.5}$CaMSN (1.3 ± 0.1 g), compared with the gauze (23.5 ± 5.7 g). The $Ga_{0.5}$CaMSN could be quickly adsorbed on the wound surface to seal the bleeding outlet and form the blood clots. The experiment showed that $Ga_{0.5}$CaMSN could significantly reduce hemostasis time and blood loss, and all the animals survived within 24 h. Therefore, $Ga_{0.5}$CaMSN is effective in fatal arterial bleeding and has the potential to be applied to wounds with acute bleeding.

5 Conclusion

In this study, the ordered mesoporous silica nanoparticles with controlled pore size and particle size doped with calcium and gallium were developed for hemorrhage and infection control. The hemostatic efficacy and antibacterial properties were evaluated through a series of tests.

The results of tests demonstrated that the obtained $Ga_{0.5}$CaMSN with optimized composition could significantly activate the intrinsic pathway of coagulation cascade, promote the blood clotting and achieve successful hemorrhage control in the mouse tail amputation model and the rabbit femoral artery model. Compared with the MSN, the improved the hemostatic efficacy might be attributed to the introduction of Ca and Ga ions. In addition, the $Ga_{0.5}$CaMSN showed antibacterial activities against *E. coli* and *S. aureus* due to the existence of gallium. Therefore, $Ga_{0.5}$CaMSN has considerable potential for use as an advanced hemostatic material. And calcium and gallium will play an important role in hemorrhage and infection control which are expected to be further studied.

Acknowledgements The authors gratefully acknowledge the support for this work from the Military Medical Innovation Project [No. 18CXZ043], Natural Sciences Foundation of China [No. 51502345], Tianjin Science and Technology Major Project Program [18ZXJMTG00070] and Tianjin Sciences Foundation [16JCQNJC03100].

Compliance with Ethical Standards

Conflict of Interest The authors declare that they have no conflict of interest.

References

1. Gordy SD, Rhee P, Schreiber MA (2011) Military applications of novel hemostatic devices[J]. Expert review of medical devices 8(1): 41–47
2. Wei S, Lixin S, Jiewei L et al (2014) Comparison of the drug for infection prevention in combat injuries between the PLA and USA armed force[J]. Journal of Pharmaceutical Practice 01:75–77
3. Pfeifer R, Tarkin IS, Rocos B, Pape HC (2009) Patterns of mortality and causes of death in polytrauma patients—has anything changed?[J]. Injury 40(9):907–911
4. Kheirabadi BS, Scherer MR, Estep JS, Dubick MA, Holcomb JB (2009) Determination of efficacy of new hemostatic dressings in a model of extremity arterial hemorrhage in swine[J]. J Trauma Acute Care Surg 67(3):450–460
5. Kheirabadi BS, Mace JE, Terrazas IB, Fedyk CG, Estep JS, Dubick MA, Blackbourne LH (2010) Safety evaluation of new hemostatic agents, smectite granules, and kaolin-coated gauze in a vascular injury wound model in swine[J]. J Trauma Acute Care Surg 68(2):269–278
6. Kheirabadi BS, Edens JW, Terrazas IB, Estep JS, Klemcke HG, Dubick MA, Holcomb JB (2009) Comparison of new hemostatic granules/powders with currently deployed hemostatic products in a lethal model of extremity arterial hemorrhage in swine[J]. J Trauma Acute Care Surg 66(2):316–328
7. Littlejohn L, Bennett BL, Drew B (2015) Application of current hemorrhage control techniques for backcountry care: part two, hemostatic dressings and other adjuncts[J]. Wilderness & environmental medicine 26(2):246–254
8. Rhee P, Brown C, Martin M, et al. QuikClot use in trauma for hemorrhage control: case series of 103 documented uses[J]. Journal of Trauma and Acute Care Surgery, 2008, 64(4): 1093-1099
9. McManus J, Hurtado T, Pusateri A et al (2007) A case series describing thermal injury resulting from zeolite use for hemorrhage control in combat operations[J]. Prehospital Emergency Care 11(1): 67–71
10. Plurad D, Chandrasoma S, Best C, Rhee P (2009) A complication of intracorporeal use of QuikClot for pelvic hemorrhage[J]. J Trauma Acute Care Surg 66(5):1482–1484
11. Wright JK, Kalns J, Wolf EA, Traweek F, Schwarz S, Loeffler CAK, Snyder W, Yantis Jr LD, Eggers J (2004) Thermal injury resulting from application of a granular mineral hemostatic agent[J]. J Trauma Acute Care Surg 57(2):224–230
12. Bennett BL, Littlejohn L Review of new topical hemostatic dressings for combat casualty care[J]. Military Medicine 179(5):497–514
13. Li F, Tian F, Liu CJ et al (2013) Advance in emergengcy hemostatic materials[J]. Materials Review 27(3):70–73
14. Clay JG, Grayson JK, Zierold D (2010) Comparative testing of new hemostatic agents in a swine model of extremity arterial and venous hemorrhage[J]. Mil Med 175(4):280–284
15. Littlejohn LF, Devlin JJ, Kircher SS, Lueken R, Melia MR, Johnson AS (2011) Comparison of Celox-a, ChitoFlex, WoundStat, and combat gauze hemostatic agents versus standard gauze dressing in control of hemorrhage in a swine model of penetrating trauma[J]. Acad Emerg Med 18(4):340–350

16. Wang C, Zhou H, Niu H, Ma X, Yuan Y, Hong H, Liu C (2018) Tannic acid-loaded mesoporous silica for rapid hemostasis and antibacterial activity[J]. Biomaterials science 6(12):3318–3331
17. Nie W, Dai X, Li D, McCoul D, Gillispie GJ, Zhang Y, Yu B, He C (2018) One-pot synthesis of silver nanoparticle incorporated mesoporous silica granules for hemorrhage control and antibacterial treatment[J]. ACS Biomaterials Science & Engineering 4(10): 3588–3599
18. Zhou H, Wang C, Niu H, Duan B, Ma X, Hong H, Yuan Y, Liu C (2018) A novel droplet-fabricated mesoporous silica-based nanohybrid granules for hemorrhage control[J]. J Biomed Nanotechnol 14(4):649–661
19. Doolittle RF (2017) The conversion of fibrinogen to fibrin: a brief history of some key events[J]. Matrix Biol 60:5–7
20. Lebrasseur N (2003) Calcium for strong clotting. J Cell Biol 160(7): 980.2
21. Kaneko Y, Thoendel M, Olakanmi O, Britigan BE, Singh PK (2007) The transition metal gallium disrupts Pseudomonas aeruginosa iron metabolism and has antimicrobial and antibiofilm activity[J]. J Clin Invest 117(4):877–888
22. Zeimaran E, Pourshahrestani S, Djordjevic I, Pingguan-Murphy B, Kadri NA, Towler MR (2015) Bioactive glass reinforced elastomer composites for skeletal regeneration: a review[J]. Mater Sci Eng C 53:175–188
23. Arnold CE, Bordin A, Lawhon SD, Libal MC, Bernstein LR, Cohen ND (2012) Antimicrobial activity of gallium maltolate against Staphylococcus aureus and methicillin-resistant S. aureus and Staphylococcus pseudintermedius: an in vitro study[J]. Vet Microbiol 155(2–4):389–394
24. Lyu YH, Li X, Liu Z et al (2018) Antimicrobial activity of gallium[J]. Chin J Antibiot 43(4):394–400
25. Xu Z, Zhao X, Chen X, Chen Z, Xia Z (2017) Antimicrobial effect of gallium nitrate against bacteria encountered in burn wound infections[J]. RSC Adv 7(82):52266–52273
26. Goodley PH, Rogosnitzky M (2011) The effect of gallium nitrate on arresting blood flow from a wound[J]. Case Rep Med 2011:1–3
27. Rogosnitzky M. Method of wound hemostasis using liquid gallium nitrate: U.S. Patent 8,652,509[P]. 2014-2-18
28. Goncalves J, Wasif N, Esposito D, Coico JM, Schwartz B, Higgins PJ, Bockman RS, Staiano-Coico L (2002) Gallium nitrate accelerates partial thickness wound repair and alters keratinocyte integrin expression to favor a motile phenotype[J]. J Surg Res 103(2):134–140
29. Bauters A, Holt DJ, Zerbib P, Rogosnitzky M (2013) Gallium nitrate induces fibrinogen flocculation: an explanation for its hemostatic effect?[J]. BioMetals 26(6):935–939
30. Chen Z, Li F, Liu C, Guan J, Hu X, du G, Yao X, Wu J, Tian F (2016) Blood clot initiation by mesoporous silica nanoparticles: dependence on pore size or particle size?[J]. J Mater Chem B 4(44):7146–7154
31. Zhang Y, Zhi Z, Jiang T, Zhang J, Wang Z, Wang S (2010) Spherical mesoporous silica nanoparticles for loading and release of the poorly water-soluble drug telmisartan[J]. J Control Release 145(3):257–263
32. Nandiyanto ABD, Kim SG, Iskandar F, Okuyama K (2009) Synthesis of spherical mesoporous silica nanoparticles with nanometer-size controllable pores and outer diameters[J]. Microporous Mesoporous Mater 120(3):447–453
33. Wu S, Huang Z, Yue J, Liu D, Wang T, Ezanno P, Ruan C, Zhao X, Lu WW, Pan H (2015) The efficient hemostatic effect of Antarctic krill chitosan is related to its hydration property[J]. Carbohydr Polym 132:295–303
34. Zhang Y, Guan J, Wu J, Ding S, Yang J, Zhang J, Dong A, Deng L (2019) N-alkylated chitosan/graphene oxide porous sponge for rapid and effective hemostasis in emergency situations[J]. Carbohydr Polym 219:405–413
35. Zhao X, Guo B, Wu H, Liang Y, Ma PX (2018) Injectable antibacterial conductive nanocomposite cryogels with rapid shape recovery for noncompressible hemorrhage and wound healing[J]. Nat Commun 9(1):2784
36. Yoshida T, Yoshioka Y, Morishita Y, Aoyama M, Tochigi S, Hirai T, Tanaka K, Nagano K, Kamada H, Tsunoda SI, Nabeshi H, Yoshikawa T, Higashisaka K, Tsutsumi Y (2015) Protein corona changes mediated by surface modification of amorphous silica nanoparticles suppress acute toxicity and activation of intrinsic coagulation cascade in mice[J]. Nanotechnology 26(24):245101
37. Lee DW, Powers K, Baney R (2004) Physicochemical properties and blood compatibility of acylated chitosan nanoparticles[J]. Carbohydr Polym 58(4):371–377